Influence of incomplete fusion on complete fusion: Observation of a large incomplete fusion fraction at $E \approx 5$–7 MeV/nucleon

Pushpendra P. Singh,* B. P. Singh,† Manoj Kumar Sharma, Unnati, Devendra P. Singh, and R. Prasad
Accelerator Laboratory, Department of Physics, A. M. University, Aligarh (UP) 202 002, India

Rakesh Kumar and K. S. Golda
NP-Group, Inter University Accelerator Center, Aruna Asaf Ali Road, P. O. Box 10502, New Delhi 110 067, India

(Received 16 April 2007; revised manuscript received 9 August 2007; published 15 January 2008)

Experiments have been carried out to explore the reaction dynamics leading to incomplete fusion of heavy ions at moderate excitation energies. Excitation functions for $^{168}Lu^{m}$, ^{167}Lu, ^{167}Yb, ^{166}Tm, ^{179}Re, ^{177}Re, ^{177}W, ^{178}Ta, and ^{177}Hf radio-nuclides populated via complete and/or incomplete fusion of ^{16}O with ^{159}Tb and ^{169}Tm have been studied over the wide projectile energy range $E_{proj} \approx 75$–95 MeV. Recoil-catcher technique followed by off-line γ-spectrometry has been employed in the present measurements. Experimental data have been compared with the predictions of theoretical model code PACE2. The experimentally measured production cross sections of α-emitting channels were found to be larger as compared to the theoretical model predictions and may be attributed to incomplete fusion at these energies. During the analysis of experimental data, incomplete fusion has been found to be competing with complete fusion. As such, an attempt has been made to estimate the incomplete fusion fraction for both the systems, and has been found to be sensitive for projectile energy and mass asymmetry of interacting partners.

DOI: 10.1103/PhysRevC.77.014607 PACS number(s): 25.70.Gh, 25.70.Jj, 25.70.Mn

I. INTRODUCTION

The reaction dynamics studies at energies near and above the Coulomb barrier (CB) with light heavy ions ($Z \leqslant 10$) and high-Z targets have been a topic of considerable interest [1–3]. Recent experimental data [4–8] at these energies indicate that the most dominating fusion processes are (a) complete fusion (CF) and (b) in-complete fusion (ICF). For incident energies up to a little above the Coulomb barrier, with the collision trajectories of input angular momentum $\ell \leqslant \ell_{crit}$, heavy ion interaction is dominated by entire linear momentum transfer from projectile to target nucleus leading to complete fusion process. As a consequence, a fully equilibrated excited compound nucleus of pre-determined charge, mass, and angular momenta is supposed to be formed via essentially a single route, after which the light nuclear particle(s) and characteristic γ-radiations are emitted as a means of deexcitation. However, at relatively high bombarding energies and for input angular momentum $\ell \geqslant \ell_{crit}$, complete fusion gradually gives way to incomplete fusion, where fractional mass and charge as well as the linear momentum of projectile are transferred to the target nucleus, due to the prompt emission of α-clusters in forward cone with almost projectile velocity. As a result of such process, projectile-like and target-like partners may come into picture in the exit channel. Such kind of reactions were first observed by Britt and Quinton [9] in the bombardment of heavy targets by ^{12}C, ^{14}N, and ^{16}O projectiles at energies well above the Coulomb barrier. Further, particle-γ coincidence studies by Inamura *et al.* [10] contributed a great deal to the understanding of underlying dynamics. Some of the important features of incomplete fusion process are (i) ICF contributes a significant fraction to the reaction cross section in case of low-Z projectiles and high-Z targets; (ii) the forward mean-ranges of recoils show relatively smaller depth in the stopping medium than that of complete fusion residues, strengthening the concept of fractional momentum transfer; (iii) the outgoing projectile-like fragments are mainly concentrated in forward cone and their energy spectrum essentially peak at the projectile velocity [9]; and (iv) the spin distribution of evaporation residues populated via incomplete fusion are found to be distinctly different as observed for complete fusion process [10,11].

In order to explain some of these features several dynamical models viz. SUMRULE model [12], Break-Up Fusion (BUF) model [13], Promptly Emitted Particles (PEP's) model [14], etc., have been proposed. The SUMRULE model of Wilczynski *et al.* [12] considers that ICF processes mainly occur in peripheral interactions and are localized in the angular momentum space above the critical angular momentum for the complete fusion. The peripheral nature of ICF has also been emphasized by Trautmann *et al.* [15] and Inamura *et al.* [16,17]. The BUF-model of Udagawa and Tamura [13] is based on the distorted wave Born approximation (DWBA) formalism for elastic breakup, where the projectile is supposed to breakup into α-clusters as it approaches the nuclear field of target nucleus. One of the fragments of projectile is assumed to fuse with target nucleus to form an incompletely fused composite system (ICF) and unfused fragment continues to move nearly undeflected or less deflected in the forward cone with almost projectile velocity. However, in PEP's model [14], the particles transferred from the projectile to target nucleus are assumed to get accelerated in the nuclear field of target nucleus and hence, acquire extra velocity to escape. Moreover, the leading-particle model of Natowitz *et al.* [18], hybrid model of Blann *et al.* [19],

*pushpendrapsingh@gmail.com; also at: NP-Group, Inter-University Accelerator Center, Aruna Asaf Ali Road, P. O. Box 10502, New Delhi 110 067, India.
†bpsinghamu@gmail.com

and Fermi-jet model [20–22] have also been proposed and seem to explain some of the experimental data related to incomplete fusion. As a matter of fact, the above existing models qualitatively explain the experimental data particularly at $E/A \geqslant 10.5$ MeV, but are not consistent at relatively low bombarding energies [10,23,24]. Moreover, during the past decade, several reports indicated the onset of incomplete fusion even at low bombarding energies, i.e., $E/A \approx 5$–7 MeV [25–29]. Parker *et al.* [30] observed forward α-particles in low-Z heavy ion interactions on ^{51}V target at $E/A \approx 6$ MeV. Morgenstern *et al.* [31] observed the velocity spectra of evaporation residues in the interaction of ^{40}Ar with boron and carbon targets. Morgenstern *et al.* [32] have also showed that, incomplete fusion reactions significantly contribute to the total reaction cross section for mass asymmetric systems as compared to mass symmetric systems at the same relative velocity. Later studies by Vineyard *et al.* [33] and Beck *et al.* [34] also supported the systematics presented by Morgenstern *et al.* [32]. However, the detailed conclusions regarding the multiplicity of linear momentum transfer, effect of mass asymmetry, role of different ℓ-bins associated with incomplete fusion processes, could not be drawn and such studies are still limited for few projectile-target combinations in medium mass region, i.e., $A \approx 150$. Moreover, the ICF reactions are considered to be a promising route to produce high spin states in heavy residues using light heavy ion beams ($A \leqslant 16$) even at low bombarding energies [35–37]. As such, in order to have better understanding of incomplete fusion dynamics, precise experimental data covering a wide range of periodic table and energies are required. The study of ICF dynamics in the framework of all these aspects may provide key parameters to determine optimum irradiation conditions for the production of radioactive ion beams (RIBs) [38,39].

In view of the availability of limited data covering only few projectile-target combinations at $E/A \approx 5$–7 MeV, our group has undertaken a program of precise measurement and analysis of excitation functions (EF's), recoil range distributions (RRD's), and spin distributions of residues populated via complete and/or incomplete fusion using particle-γ coincidence technique for various projectile-target combinations over a wide projectile energy range. As a part of ongoing programme to explore the dynamics of light heavy ion induced reactions (mainly complete and incomplete fusion), excitation functions for a large number of residues produced in several projectile-target combinations have been measured [27,40,41]. The present work deals with the extension of our earlier observations and a part of the analysis of these systems have already been published [40–42]. In this work, the influence of incomplete fusion on complete fusion has been studied and cross sections for nine radio-nuclides populated in ^{16}O+^{159}Tb and ^{16}O+^{169}Tm systems have been presented. The present paper is organized as follows. The experimental details and the evaporation residues identification are given in Sec. II. The experimentally measured EFs for both the systems have been compared with the predictions of statistical model code PACE2 and detailed analysis is given in Sec. III. The influence of incomplete fusion on complete fusion has been studied by the deduction of incomplete fusion fraction calculated on the lines of Gomes *et al.* [54] and the detailed discussion is given in Sec. IV. Section V deals with the summary and conclusions of the present work.

II. EXPERIMENTAL DETAILS

The experiments were carried out at the Inter-University Accelerator Center (IUAC), New Delhi, India using 15-UD Pelletron Accelerator facilities. A brief description of experimental details, such as target preparation and irradiations, post irradiation analysis, identification of evaporation residues, etc., are presented in the following subsections.

A. Target preparation

The self-supporting ^{159}Tb (abundance = 99.99%) targets of thickness $\approx$0.83 mg/cm^2 were prepared by rolling method and the ^{169}Tm (abundance = 100%) targets of $\approx$0.65 mg/cm^2 thickness were deposited on Al-backing of $\approx$1.5 mg/cm^2 thickness, using vacuum-evaporation technique. The Al-backing of ^{169}Tm targets served as energy degrader as well as catcher foil during the irradiations. The ^{159}Tb targets were backed by thick Al-catchers of $\approx$2 mg/cm^2 thickness to trap the recoiling nuclei. Since, a precise knowledge of the target thickness is an essential part of the absolute cross-section measurement of different reaction products, therefore, the thickness of each target was determined by α-transmission method. This technique is based on the measurement of the energy loss per unit path length by 5.487 MeV α-particles obtained from standard ^{241}Am source, while passing through the material of target. The targets were cut into the size of 1.2 $\times$ 1.2 cm^2 and were pasted on Al-holders having concentric hole of 1.0 cm diameter. The Al-holders were used for rapid dissipation of heat produced during the irradiations.

B. Irradiations

The irradiations have been carried out in the general purpose scattering chamber (GPSC) having an invacuum transfer facility (ITF) using conventional recoil-catcher technique. The ITF has been used to minimise the time lapse between the stop of irradiations and beginning of the counting. Two stacks each containing four and five samples of ^{159}Tb were irradiated at beam energies $\approx$87 and 95 MeV, while, two stacks of ^{169}Tm targets having four and three samples each were irradiated at energies $\approx$92 and $\approx$95 MeV by an $^{16}O^{7+}$ beam. The beam current was monitored $\approx$30–50 nA for both the systems in all irradiations. The targets along with Al-catcher foils were placed normal to the beam direction so that the recoiling nuclei, which have been populated during the interaction of projectile and target nuclei may be trapped in the catcher foil thickness. Keeping in view the half-lives of interest, irradiations have been carried out for $\approx$8–10 h. The beam flux was calculated by the total charge collected in the Faraday cup, placed behind the target-catcher foil assembly, using a current integrator device.

C. Post irradiation analysis

After the irradiation the stack of targets along with catcher foils was taken out from the GPSC with the help of an ITF. The evaporation residues populated in each target-catcher foil assembly via complete and/or incomplete fusion of ^{16}O

were identified by counting the induced activities using high resolution HPGe γ-ray spectrometer of 100 c.c. active volume coupled to PC through CAMAC based FREEDOM software. The energy and efficiency calibration of γ-spectrometer has been done using various standard γ-radiation sources of known strength. Further, the spectrometer resolution was $\approx$2 keV for 1.33 MeV γ-ray of ^{60}Co source. In the present work, the standard γ-sources and the irradiated samples were counted in the same geometry to keep the geometry dependent detector efficiency same for both. The geometry dependent efficiency ($G\varepsilon$) of HPGe γ-ray spectrometer for different source-detector separation was estimated using following relation:

$$G\varepsilon = \frac{N_o}{N_{ao}\,\theta\,e^{(-\lambda t)}}, \tag{1}$$

where N_o is the observed disintegration rate of the standard γ-source at the time of measurement, N_{ao} is the disintegration rate at the time of manufacture, λ is the decay constant, t is the lapse time between the manufacture of the source and start of counting, θ is the branching ratio of the characteristic γ-rays. Attention was paid to keep the dead time of the detector $\leqslant$10% by suitably adjusting the source-detector separations. Keeping in view the half-lives of interest, the counting of activities induced in the samples were performed for a considerably long period.

D. Identification of evaporation residues

As already discussed, the evaporation residues populated via different reaction processes are likely to decay to the ground state by emitting characteristic γ-radiations, whose detection is an unique way for their identification. Thus, the observed intensity of the induced activities is a measure of production probability of evaporation residues. The γ-ray spectra of individual target-catcher foil assembly were recorded at the increasing times. The typical γ-ray spectra of ^{159}Tb and ^{169}Tm samples irradiated by $^{16}O^{7+}$ at $\approx$95 MeV are shown in Figs. 1 and 2. The various peaks in observed γ-ray

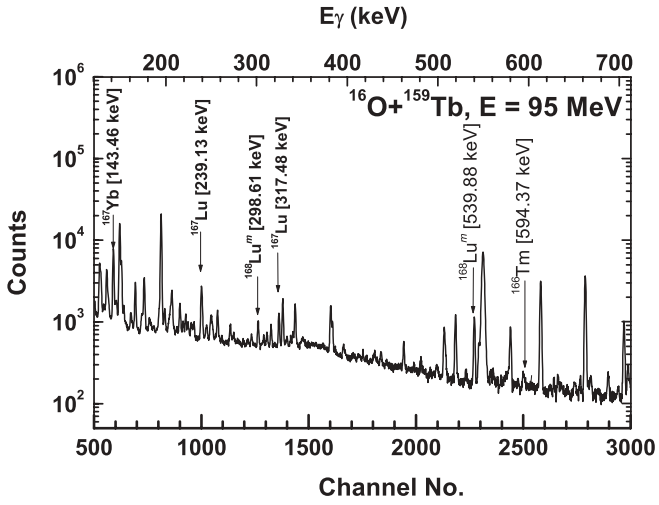

FIG. 1. Typical γ-ray spectra showing γ-lines of different radionuclides populated via CF and/or ICF in ^{16}O+^{159}Tb system at projectile energy $\approx$95 MeV.

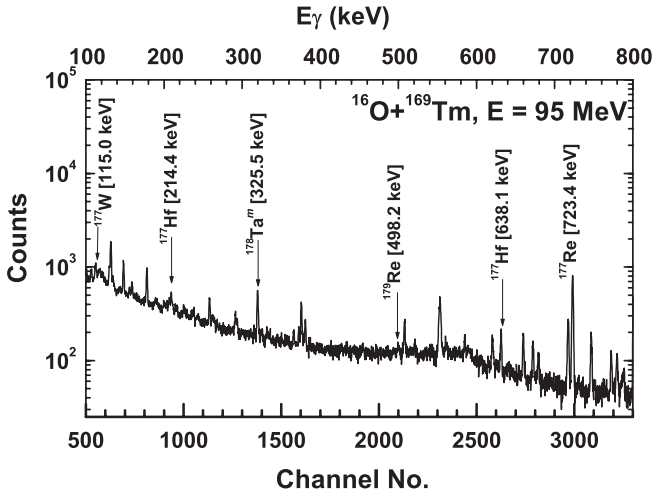

FIG. 2. Typical γ-ray spectra showing γ-lines of different radionuclides populated via CF and/or ICF in ^{16}O+^{169}Tb system at projectile energy $\approx$95 MeV.

spectra were assigned to the different evaporation residues. The reaction products were identified not only by the energy of the characteristic γ-radiations but also by the measured half-lives of residues. The measured half-lives of evaporation residues were found to be in good agreement with the literature values. Data analysis have been performed using FREEDOM software for nuclear data analysis. Area under the peaks of identified γ-lines of evaporation residues were used to estimate the count rate followed by production probability measurement. Nuclear data like half-lives, γ-ray energies, etc., have been taken from the Table of Isotopes [45] and Nuclear Wallet Card [43]. Identified evaporation residues along with their spectroscopic properties are given in Tables I and II.

E. Determination of production cross sections

A change in the composition of the target nucleus takes place, as a result of different reaction processes forming the evaporation residues, which may be identified on the basis their half-lives and characteristics γ-radiations. The intensities of the characteristic γ-radiations were used to estimate the reaction cross sections. A FORTRAN program EXP-SIGMA based on the following formulation has been used for the

TABLE I. List of identified evaporation residues produced in ^{16}O+^{159}Tb system via complete and/or in-complete fusion.

Reactions	Residues	E_γ (keV)	half-life	J_π	a_γ (%)
^{159}Tb(^{16}O,$\alpha 3n$)	$^{168}_{71}$Lu^{m}	298.61	6.7 min	3+	17
		539.88			47
^{159}Tb(^{16}O,$\alpha 4n$)	$^{167}_{71}$Lu	239.13	57.5 min	7/2+	8.2
		317.48			1.5
^{159}Tb(^{16}O,$\alpha p 3n$)	$^{167}_{70}$Yb	143.46	17.5 min	5/2−	2.10
^{159}Tb(^{16}O,$2\alpha n$)	$^{166}_{69}$Tm	594.37	7.7 h	2+	3.08
		1176.68			8.4

TABLE II. List of identified evaporation residues produced in $^{16}O+^{169}Tm$ system via complete and/or in-complete fusion.

Reactions	Residues	E_γ (keV)	Half-life	J_π	a_γ (%)
$^{169}Tm(^{16}O,\alpha p3n)$	$^{177}_{74}W$	115.0	2.21 h	1/2−	59
		426.94			13.1
$^{169}Tm(^{16}O,\alpha 2pn)$	$^{178}_{73}Ta$	325.5	2.36 h	7−	94.1
		331.6			32
$^{169}Tm(^{16}O,\alpha 3pn)$	$^{177}_{72}Hf$	214.4	51.4 min	7/2−	8.3
		638.1			20.0
$^{169}Tm(^{16}O,\alpha 4n)$	$^{177}_{75}Re$	1118.4	14.0 min	5/2−	25
		723.4			15
$^{169}Tm(^{16}O,\alpha 2n)$	$^{179}_{75}Re$	221.9	19.5 min	5/2+	3.6
		401			7.3
		498.2			5.7

determination of the production cross sections of evaporation residues [44],

$$\sigma_r = \frac{C_{t=0}}{N_0\theta\phi G_\varepsilon K[1-\exp(-\lambda t_1)]}, \tag{2}$$

where $C_{t=0}$ is the total number of observed counts at the time of stop the irradiation, N_0 is the initial number of target nuclei, θ is the branching ratio of the characteristic γ-ray, ϕ is the flux of incident beam, G_ε is the geometry dependent efficiency of the spectrometer for a particular γ-ray energy, and $K = [1-\exp(-\mu d)]/\mu d$ is the self-absorption correction factor for the material of the sample of thickness d (gm/cm^2) and of absorption coefficient μ (cm^2/gm). The factor $[1-\exp(-\lambda t_1)]$ is a saturation correction factor. In the present work, excitation functions for nine evaporation residues $^{168}Lu^m(\alpha 3n)$, $^{167}Lu(\alpha 4n)$, $^{167}Yb(\alpha p3n)$, and $^{166}Tm(2\alpha n)$ produced in $^{16}O+^{159}Tb$ system, and $^{179}Re(\alpha 2n)$, $^{177}Re(\alpha 4n)$, $^{177}W(\alpha p3n)$, $^{178}Ta(\alpha 2pn)$, and $^{177}Hf(\alpha 3pn)$ produced in $^{16}O+^{169}Tm$ system have been measured. The measured cross sections of identified evaporation residues are presented in Tables III and IV.

The errors in the measured production cross-sections may arise mainly because of (i) the nonuniform thickness of samples that may lead to the uncertainty in the determination of the number of target nuclei. To check the uniformity of the sample, thickness of the each sample was measured at different positions by α-transmission method. It is estimated that the error in the thickness of the sample material is less than 1%. (ii) Fluctuations in the beam current may result in the variation of incident flux, proper care has been taken to keep the beam current constant as far as possible and, correction in flux determination from the fluctuation in beam current has been applied. (iii) Uncertainity in the determination of geometry dependent spectrometer efficiency. The error in the efficiency determination due to the statistical fluctuations in counts is estimated to be less than 2%. (iv) The losses of the product nuclei recoiling out of the sample may introduce large errors in the measured cross sections. The thickness of the catcher foils was sufficient to stop even the most energetic residues, moreover, in the present measurements both the sample and the catcher foils were counted together and hence, the losses due to the recoiling of nuclei is avoided. (v) The dead time of the spectrometer was kept $\leqslant$10% by suitably adjusting sample-detector distance. These errors exclude the uncertainty of the nuclear data such as branching ratio, decay constant, etc., which have been taken from the Table of Isotopes [45]. The overall errors from these factors including statistical error are estimated to be $\leqslant$15%.

TABLE III. Experimentally measured production cross sections for evaporation residues populated via ICF and/or CF in $^{16}O+^{159}Tb$ system along with the projectile energies.

Lab energy (MeV)	σ ($^{168}Lu^m$) (mb)	σ (^{167}Lu) (mb)	σ (^{167}Yb) (mb)	σ (^{166}Tm) (mb)
75.2 ± 0.9	3 ± 0.59	–	–	–
78.7 ± 0.9	12 ± 1.86	–	–	1.93 ± 0.36
83.2 ± 0.9	57 ± 6.81	5 ± 1.12	9 ± 1.23	7 ± 1.24
87.2 ± 0.8	69 ± 9.8	46 ± 6.54	28 ± 4.22	28 ± 3.11
89.6 ± 1.0	87 ± 11.67	59 ± 9.61	49 ± 5.94	31 ± 5.69
94.6 ± 0.4	145 ± 16.93	118 ± 17.52	21 ± 3.63	49 ± 7.56

III. DATA ANALYSIS: STATISTICAL MODEL CALCULATIONS WITH PACE2

In order to examine the extent to which the observed quantities are described in terms of the equilibrated decay of $^{175}Ta^\star$ and $^{185}Ir^\star$ populated in the interaction of ^{16}O with ^{159}Tb and ^{169}Tm within the energy range $E \approx 75$–95 MeV, the presently measured excitations functions have been compared with those calculated using statistical model code PACE2 (based on Hauser-Feshbach theory) [46]. The code PACE2 is based on statistical approach of CN deexcitation by Monte Carlo procedure. The angular momentum projections are calculated at each stage of deexcitation. The angular momentum conservation is explicitly taken into account at each step, and the CF cross sections are calculated using BASS formula [47].

The partial cross section (σ_ℓ) for the formation of compound nucleus at a particular angular momentum ℓ and specific bombarding energy, E is given by

$$\sigma_\ell = \frac{\lambda^2}{4\pi}(2\ell+1)T_\ell, \tag{3}$$

where λ is reduced wavelength and the transmission coefficients T_ℓ may be given by the expression

$$T_\ell = \left[1+\exp\left(\frac{\ell-\ell_{\max}}{\Delta}\right)\right]^{-1}, \tag{4}$$

where Δ is the diffuseness parameter and $\ell_{\max}$ the maximum amount of ℓ detained by total fusion cross section,

$$\sigma_F = \sum_{\ell=0}^{\infty}\sigma_\ell. \tag{5}$$

The optical model potentials of Becchetti and Greenlees [48] are used for calculating the transmission coefficients for

TABLE IV. Experimentally measured production cross sections for evaporation residues populated via ICF and/or CF in $^{16}O+^{169}Tm$ system along with the projectile energies.

E_{beam} (MeV)	σ_{cum} (^{177}W) (mb)	σ_{ind} (^{177}W) (mb)	σ (^{178}Ta) (mb)	σ (^{177}Hf) (mb)	σ (^{177}Re) (mb)	σ (^{179}Re) (mb)
74.9 ± 0.9	–	–	–	–	–	3 ± 0.89
78.7 ± 0.9	17 ± 2.49	–	36 ± 4.58	8 ± 0.89	–	14 ± 1.24
82.0 ± 0.8	41 ± 4.3	35 ± 3.17	87 ± 8.91	11 ± 1.27	5 ± 1.09	19 ± 3.02
85.8 ± 0.8	36 ± 5.9	28 ± 4.63	106 ± 7.61	28 ± 2.32	7 ± 1.04	39 ± 4.64
88.9 ± 1.0	73 ± 6.2	58 ± 5.31	143 ± 13.57	37 ± 2.59	13 ± 1.96	46 ± 5.36
91.6 ± 0.4	79 ± 8.3	62 ± 6.48	149 ± 12.81	40 ± 3.71	15 ± 2.97	37 ± 6.98
94.6 ± 0.4	96 ± 9.5	61 ± 7.19	194 ± 18.41	63 ± 6.51	31 ± 3.17	32 ± 3.71

neutron and proton, and optical model potential of Satchler [49] is used for α-particle emissions. In the description of γ-ray competitions, emission of $E1$, $E2$, $M1$, and $M2$ γ-ray are included and the γ-rays strength for different transitions, are taken from tables of Endt [50]. In this code, the level density parameter $a(=A/K)$, is one of the important parameters, where, A is the mass number of the nucleus and K is a free parameter. The value of K may be varied to match the experimental data. In the present work, we tested the experimental data using different values of level density parameters from $A/11$ to $A/8$ MeV^{-1}. As a representative case, the effect of the variation of above parameter 'K' on calculated EF's for the population of Lu isotopes via CF and/or ICF in $^{16}O+^{159}Tb$ system is shown in Figs. 3(a) and 3(b). As can be observed from this figure, the theoretical predictions with different input parameters are almost similar or a very small change comes into picture for higher value of level density parameter at relatively higher projectile energies. It may, however be pointed out that a value of $K \geqslant 10$, may give rise to the anomalous effect in particle multiplicity, and compound nucleus temperature [51]. Though, it is possible to explain all the excitation functions with different values of parameters of the code for individual channels, however, from the physics point of view, it is quite unreasonable. As such, in the present work all the calculations have been performed consistently using same set of parameters for all the channels. The value of level density parameter (a) was taken as $A/8$ MeV^{-1}, i.e., $K = 8$, as suggested by Gilbert and Cameron [52]. This set of parameters reproduced the excitation functions for complete fusion channels satisfactorily, as mentioned in our earlier publications [40,41]. This further shows that the optical model parameters used in these calculations are satisfactory. It may, however, be pointed out that the ICF process is not taken into account in code PACE2. Hence, the enhancement of experimentally measured production cross sections as compared to the theoretical predictions may be attributed to the incomplete fusion process.

A. Excitation functions: $^{16}O+^{159}Tb$ system

In Figs. 3 and 4, the experimentally measured and theoretically calculated excitation functions for four radio-nuclides $^{167,168}Lu^{m}$, ^{167}Yb, and ^{166}Tm produced in $^{16}O+^{159}Tb$ system in the energy range ≈70–95 MeV are shown. The reaction products $^{167,168}Lu^{m}$ have ground and metastable states of half-lives 51.5 min and 6.7 min, respectively. The reaction products $^{167,168}Lu^{m}$ may be formed both via complete and/or incomplete fusion of ^{16}O with ^{159}Tb. In case of complete fusion, composite system $^{175}Ta^{*}$ is formed, which may decay via the emission of an α-particle and three or four neutrons leaving behind the above residues. The same residues may also be populated via ICF, it can be explained by assuming the breakup of ^{16}O-nucleus into its fragments viz. ^{12}C and ^{4}He (α-particle) in the nuclear force field of target nucleus. One of the fragments ^{12}C fuses with ^{159}Tb, forming an incompletely fused composite system $^{171}Lu^{*}$, which may decay by the emission of three neutrons forming $^{168}Lu^{m}$ and four neutrons forming ^{167}Lu. Similarly, the reaction product ^{167}Yb, which has ground state of half-life 17.5 min, is expected to be populated via

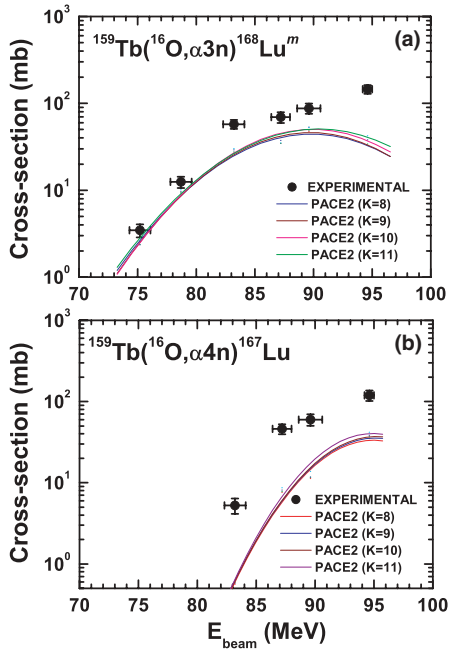

FIG. 3. (Color online) Experimentally measured and theoretically calculated excitation functions for $^{167,168}Lu^{m}$ isotopes, expected to be populated via $\alpha 4n$ and $\alpha 3n$ channels in $^{16}O+^{159}Tb$ system. The dark circles indicates the experimental data points and the solid lines represents the polynomial fit to the PACE2 predictions at different input parameters.

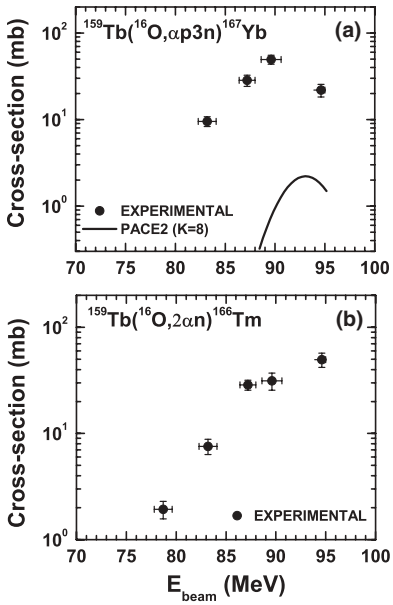

FIG. 4. Experimentally measured and theoretically calculated excitation functions for (a) ^{167}Yb populated via $\alpha p3n$ channel, and (b) ^{166}Tm populated via $2\alpha n$ channel in interaction ^{16}O+^{159}Tb system. Sold lines represents the PACE2 predictions. For ^{166}Tm residue, the theoretical predictions found to negligible and hence, not plotted in the figure.

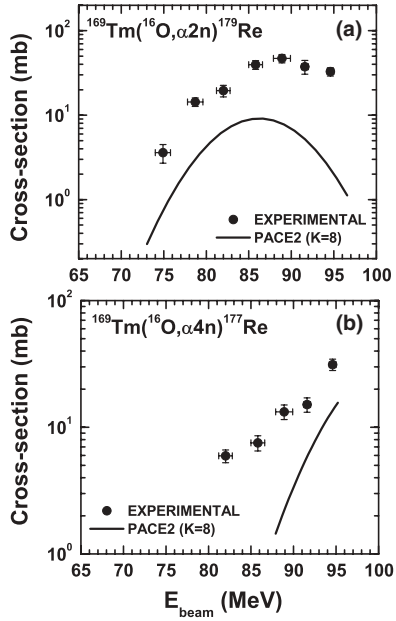

FIG. 5. Experimentally measured and theoretically calculated EF's for ^{177,179}Re isotopes expected to be populated via $\alpha 4n$ and $\alpha 2n$ in ^{16}O+^{169}Tm system. Explanation of symbols is the same as in Figs. 3 and 4.

complete fusion ($\alpha p3n$) channel and/or incomplete fusion (i.e., the fusion of ^{12}C with ^{159}Tb) followed by subsequent emission of one proton and three neutrons from ^{171}Lu*. The remaining α-fragment (^{4}He) of the incident ion is assumed to go on moving with beam velocity in forward direction without any significant interaction with target nucleus. Similarly, the evaporation residue ^{166}Tm ($t_{1/2} = 7.7$ h), is expected to be populated via fusion of ^{8}Be and subsequent emission of one neutron from ^{167}Tm*. However, the remaining part ^{8}Be (two α-particles) behaves like a spectator. It may be observed from Fig. 3(a), the experimentally measured cross sections are almost matching with PACE2 calculations in the energy range ≈75–80 MeV. However, in the higher energy region the measured cross sections are some what under predicted by PACE2 calculations. This may be explained by assuming that only complete fusion contributes to the formation of ^{168}Lu^m in the energy range ≈75–80 MeV, while, as the energy increases both complete and incomplete fusion contribute to the production probability. In the similar way, the theoretical values of cross-sections for most of the α-emitting channels are found to be some what underpredicted than that of experimental data, as indicated in Figs. 3(a), 3(b), and 4(a). Since, ICF is not taken into consideration in code PACE2, therefore, substantially large cross sections (in case of ^{167,168}Lu^m and ^{167}Yb evaporation residues) as compared to the theoretical ones cannot be the uncertainty in measurement and hence may be attributed to the contribution coming from incomplete fusion process of the type

$$^{16}\mathrm{O}(^{12}\mathrm{C} + {}^4\mathrm{He}) \Rightarrow {}^{12}\mathrm{C} + {}^{159}\mathrm{Tb} \Rightarrow {}^{171}\mathrm{Lu}^* + {}^4\mathrm{He}$$

(α as spectator).

Further, in case of reaction product ^{166}Tm($2\alpha n$), the theoretical predictions of PACE2 give an almost negligible cross section and hence are not shown in Fig. 4(b). This indicates that the major contribution for the population of ^{166}Tm comes from incomplete fusion process of the type

$$^{16}\mathrm{O}(^8\mathrm{Be} + {}^8\mathrm{Be}) \Rightarrow {}^8\mathrm{Be} + {}^{159}\mathrm{Tb} \Rightarrow {}^{167}\mathrm{Tm}^* + {}^8\mathrm{Be}$$

(beryllium as spectator).

B. Excitation functions: ^{16}O+^{169}Tm system

The excitation functions for five radio-nuclides ^{177,179}Re, ^{177}W, ^{178}Ta, and ^{177}Hf populated in the interaction of ^{16}O with ^{169}Tm within the energy range ≈75–95 MeV are shown in Figs. 5 and 6. As already indicated in the earlier section, the above residues may be populated via complete and/or incomplete fusion of ^{16}O with ^{169}Tm. The production of these residues leading to α-emission channels may also be explained in terms of the breakup of ^{16}O into ^{12}C and ^{4}He followed by fusion of ^{12}C with ^{169}Tm forming an incompletely fused composite system ^{181}Re*. The reaction products ^{177,179}Re, having half-lives of 14 min and 19.7 min, are expected to be populated via the emission of four and two neutrons from ^{181}Re*. Thus, the evaporation residues ^{177}Re and ^{179}Re may not only be populated via incomplete fusion but may have significant probability of being formed via complete fusion of the projectile leading to the formation of ^{185}Ir*, which may decay by the emission of two and four neutrons along with an α particle. The complete fusion component calculated by PACE2 code is shown in Fig. 5 by solid lines. As can be seen from these figures, the calculated cross-section values by PACE2 have lower magnitudes than the experimental data, which indicates the contribution from incomplete fusion at these

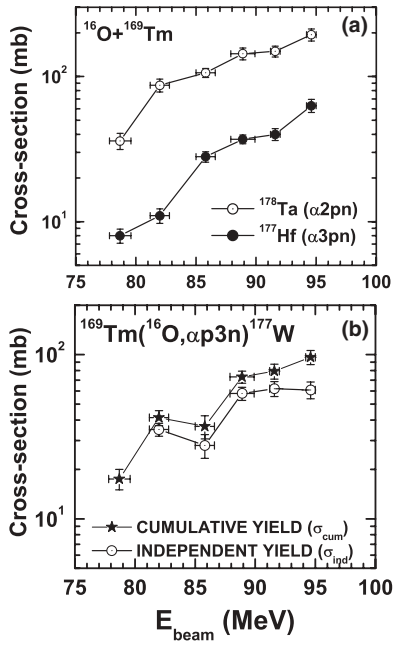

FIG. 6. Experimentally measured excitation functions for (a) ^{178}Ta and ^{177}Hf, (b) ^{177}W, evaporation residues expected to be populated via, respectively, $\alpha 2pn, \alpha 3pn$, and $\alpha p3n$ channels in ^{16}O+^{169}Tm system. The theoretical predictions are found to be negligible for these residues and hence are not shown in this figure. The different lines are drawn to guide the eye to the experimental data points. In (b) open circles indicate the independent yield of ^{177}W and cumulative yield is represented by solid stars.

energies. Similarly, the reaction products ^{178}Ta and ^{175}Hf have half-lives 2.45 h and 51.4 min, respectively and are expected to be populated via $\alpha 2pn$ and $\alpha 3pn$ channels, respectively, in which α-particle behaves as spectator. Since, the theoretical predictions of code PACE2 are negligible in case of ^{177}W, ^{178}Ta, and ^{177}Hf residues, and are therefore not shown in the Fig. 6(a) and 6(b). As such, it may be inferred that the major contribution to these reaction channels come from incomplete fusion processes of the type

$$^{16}\mathrm{O}(^{12}\mathrm{C} + ^{4}\mathrm{He}) \Rightarrow ^{12}\mathrm{C} + ^{169}\mathrm{Tm} \Rightarrow ^{181}\mathrm{Re}^{*} + ^{4}\mathrm{He}$$

(α as spectator).

The evaporation residue ^{177}W (half-life of 2.21 h) may be populated via three different reaction channels; (a) complete fusion of ^{16}O, i.e.,

$$^{16}\mathrm{O} + ^{169}\mathrm{Tm} \Rightarrow ^{185}\mathrm{Ir}^{*} \Rightarrow ^{177}\mathrm{W} + \alpha + p + 3n;$$

(b) incomplete fusion of ^{16}O, i.e.,

$$^{16}\mathrm{O}(^{12}\mathrm{C} + ^{4}\mathrm{He}) + ^{169}\mathrm{Tm} \Rightarrow ^{181}\mathrm{Re}^{*} + ^{4}\mathrm{He(spectator)}^{181}\mathrm{Re}^{*} \Rightarrow ^{177}\mathrm{W} + p + 3n;$$

and, (c) β^{+} emission and/or EC decay of higher charge precursor, i.e.,

$$^{16}\mathrm{O} + ^{169}\mathrm{Tm} \Rightarrow ^{177}\mathrm{Re}^{*} + ^{4}\mathrm{He} + 4n$$
$$^{177}\mathrm{Re}^{*} \Rightarrow ^{177}\mathrm{W} + \beta^{+}/\mathrm{EC}.$$

Since, the theoretical calculations (PACE2) for the CF channel '(a)' give negligible cross sections [and hence are not shown in Fig. 6(b)], it may be assumed that the residue ^{177}W is populated predominantly via ICF [channel '(b)'] and the precursor decay [channel '(c)']. Since, ^{177}W is populated via ICF and precursor decay, hence, an attempt has been made to separate out the contribution due to the precursor decay from the cumulative activity of ^{177}W. Brief details of the method used for separating precursor contribution are given here [8]

$$\sigma_{\mathrm{cum}} = \sigma_{\mathrm{ind}} + F_{\mathrm{pre}}\sigma_{\mathrm{pre}}, \tag{6}$$

where; σ_{cum} and σ_{ind} represent, respectively, the cumulative and independent yield of the residue, σ_{pre} stands for the independent contribution of the precursor. The value of precursor fraction (F_{pre}) depends on the branching ratio P_p for precursor decay to the residue and is given by

$$F_{\mathrm{pre}} = P_p \frac{T_{\mathrm{ind}}^{1/2}}{T_{\mathrm{ind}}^{1/2} - T_{\mathrm{pre}}^{1/2}}, \tag{7}$$

here, $T_{\mathrm{ind}}^{1/2}$ and $T_{\mathrm{pre}}^{1/2}$ are the half-lives of the precursor and the daughter residues, respectively. This cumulative cross section is given by

$$\sigma_{\mathrm{cum}} = \sigma_{\mathrm{ind}} + P_p \frac{T_{\mathrm{ind}}^{1/2}}{T_{\mathrm{ind}}^{1/2} - T_{\mathrm{pre}}^{1/2}}\sigma_{\mathrm{pre}}. \tag{8}$$

The values of branching ratios and the half-lives required for obtaining the coefficient F_{pre} are taken from Refs. [42,44]. Using the above formulation, in the present case, the cumulative yield (σ_{cum}) and independent yield (σ_{ind}) for ^{177}W are related as follows:

$$\sigma_{\mathrm{cum}}(^{177}\mathrm{W}) = \sigma_{\mathrm{ind}}(^{177}\mathrm{W}) + 1.118\sigma_{\mathrm{pre}}(^{177}\mathrm{Re}), \tag{9}$$

where, $\sigma_{\mathrm{pre}}(^{177}\mathrm{Re})$ is the independent yield of the precursor. As such, the precursor contribution of ^{177}W at different energies has been subtracted from cumulative yield for the determination of independent yield. The measured cumulative cross sections (σ_{cum}) as well as independent cross sections (σ_{ind}) for ^{177}W residue deduced in such a way are given in Table IV and are also plotted in Fig. 6(b). As can be seen from this figure, the precursor (^{177}Re) of ^{177}W contributes a finite value of yield to the production of ^{177}W. Moreover, the precursor (^{177}Re) starts contributing to the production probability at ≈82 MeV, which is found to increase with projectile energy. It may, however, be pointed out that the cumulative and independent yields of ^{177}W reaction product are almost same up to ≈87 MeV (within the error bars), which indicates a small contribution from the precursor for the energies up to ≈87 MeV, while as the energy increases the precursor contribution increases as inferred from the data points at ≈95 MeV. As shown in the figure, the solid stars represent the cumulative cross section of the residue ^{177}W, while the open circles represent the independent yield of this residue. A closer look at Fig. 6(b) indicates that σ_{cum} for ^{177}W and σ_{ind} for the independent production of ^{177}W have cross sections with a very small difference at lower energies. However, as one moves toward the relatively higher energy the difference also increases to a sizable value, indicating the influence of precursor contribution in this case.

Although, it may not be possible to directly obtain the relative contribution of complete and incomplete fusion from

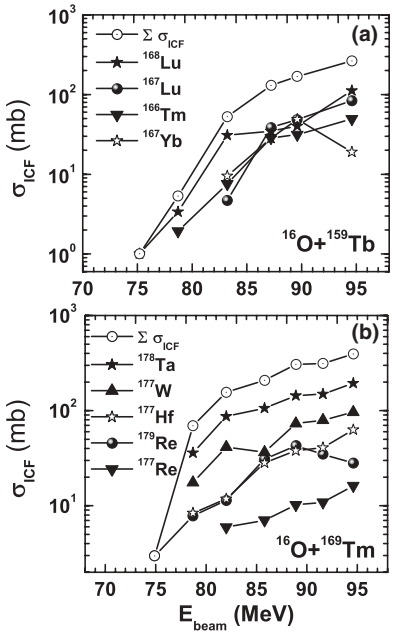

FIG. 7. Deduced incomplete fusion contribution as a function of projectile energy for (a) ^{16}O+^{159}Tb and (b) ^{16}O+^{169}Tm systems. Open circles represent the sum of all incomplete fusion channels ($\Sigma\sigma_{\rm ICF}$). Data points are connected using lines just to guide the eye.

the measurement of excitation functions, however, an attempt has been made to obtain the incomplete fusion contribution. The production cross sections which have been measured experimentally may be attributed to the both complete and/or incomplete fusion. As already mentioned, the enhancement in the experimentally measured production cross sections than that of PACE2 predictions may be attributed to incomplete fusion processes. As such, the incomplete fusion contribution for individual channels has been deduced by subtracting complete fusion cross sections ($\sigma_{\rm CF}$) (obtained by PACE2) from the experimentally measured cross sections ($\sigma_{\rm EXP}$) at respective projectile energies, as suggested by Gomes *et al.* [54]. The incomplete fusion contributions ($\sigma_{\rm ICF}$) deduced as mentioned in Ref. [54] for presently measured evaporation residues are plotted in Figs. 7(a) and 7(b) along with the sum of all incomplete fusion channels ($\Sigma\sigma_{\rm ICF}$) as a function of projectile energy. The lines drawn in these figures are just to guide the eyes. As can be seen from these curves, in general, the incomplete fusion contribution increases with projectile energy, which is expected as the break-up probability of the incident ion significantly increases with projectile energy.

In the present work, the cross sections for CF and/or ICF channels have also been calculated using the SUMRULE model [12], which is based on the generalized concept of critical angular momentum as already discussed in Sec. I. In these calculations, it is assumed that ICF channels open only for those partial waves which have ℓ-values $\geqslant \ell_{\rm crit}$. On the other hand partial waves with $\ell \leqslant \ell_{\rm crit}$, contributes to CF process. In these calculations, the input parameters such as temperature (T) of the contact zone of interacting partners, the diffuseness parameter (Δ) of transmission probability distribution (T_ℓ), and the Coulomb interaction radius (R_c) are taken as 3.5 MeV, 1.7 unit of angular momentum, and 12 fm, respectively, as suggested by Wilczynski *et al.* [12]. In the present work, it has been observed that the experimental cross section for fusion-evaporation channels agree reasonably well with the predictions of the SUMRULE model. However, there is a large discrepancy between measured and calculated cross-section values for ICF channels. As a typical example for ICF channels producing Lu isotopes in ^{16}O+^{159}Tb system, and Re isotopes in ^{16}O+^{169}Tm system, the SUMRULE calculations are lower by a factor of more than 100 in general. Similar discrepancy has also been observed in case of ^{13}C+^{181}Ta system studied by Babu *et al.* [53] in their experiment at projectile energy $\approx$6 MeV/nucleon. As a matter of fact, Wilczynski *et al.* [12] tested the SUMRULE model for the reactions at 8–10 MeV or higher energies and found satisfactory agreement in calculated and experimental cross sections. One of the possible reasons for the above disagreement in case of ICF channels in case of present measurements may be the non-validity of the generalized concept of critical angular momentum at energies with in the range of $\approx$5–7 MeV/nucleon. Further, the cluster structure of incident ion may also play an important role in ICF reactions.

IV. INCOMPLETE FUSION FRACTION ($F_{\rm ICF}$)

As already mentioned in the earlier section, the sum of all incomplete fusion components is taken as the total incomplete fusion contribution ($\Sigma\sigma_{\rm ICF}$). The contribution coming from all incomplete fusion channels ($\Sigma\sigma_{\rm ICF}$) and the sum of all complete fusion channels ($\Sigma\sigma_{\rm CF}$) obtained from PACE2 calculations are plotted along with the total fusion cross section ($\sigma_{\rm TF} = \Sigma\sigma_{\rm CF} + \Sigma\sigma_{\rm ICF}$) for presently studied systems ^{16}O+^{159}Tb and ^{16}O+^{169}Tm in Figs. 8(a) and 8(b). As can be observed from these figures, the CF component has measurable contribution even at $\approx$70 MeV, while ICF contribution seems to start from $\approx$75 MeV, in the case of presently studied systems. Further, as can be observed from Figs. 8(a) and 8(b), the separation between the plots for $\Sigma\sigma_{\rm TF}$ (solid stars) and $\sigma_{\rm CF}$ (solid circles) increases with projectile energy, which indicates that the ICF contributes larger production yield at relatively high projectile energies. This may be on account of the increasing probability of the break-up of incident ion into α-clusters (^{12}C+α and/or ^{8}Be+^{8}Be) as the projectile energy increases. It may, however, be pointed out that the difference between the plots for $\Sigma\sigma_{\rm CF}$ (solid stars) and $\sigma_{\rm TF}$ (solid circles) is more for ^{16}O+^{169}Tm system as compared to ^{16}O+^{159}Tb system at different energies. It may be because of the fact that, ^{16}O+^{169}Tm system is more mass asymmetric as that of ^{16}O+^{159}Tb system, indicating the dependence of underlying process on mass asymmetry of interacting partners. Further, the data seems to support the sensitiveness of incomplete fusion on projectile energy and mass asymmetry of interacting partners, as inferred by Morgenstern *et al.* [56]. An attempt has been made to investigate the affect of above variables on the relative contributions of complete and incomplete fusion fraction. The percentage incomplete fusion fraction ($F_{\rm ICF}$) for both the systems has been estimated from the experimentally

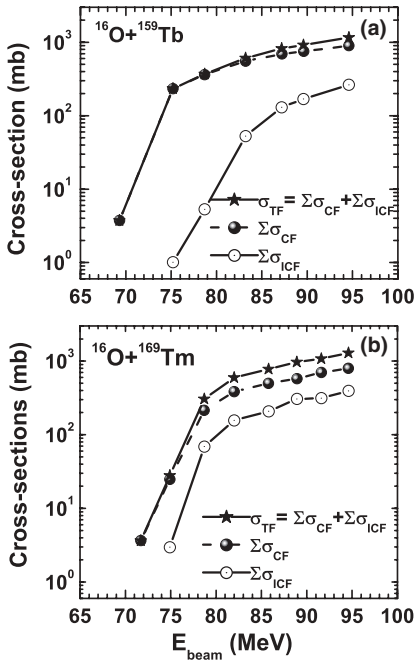

FIG. 8. Total fusion probability (σ_{TF}) along with the sum of complete ($\Sigma\sigma$CF) and incomplete fusion contributions ($\Sigma\sigma_{ICF}$) at different energies for (a) ^{16}O+^{159}Tb and (b) ^{16}O+^{169}Tm systems.

measured production cross sections as given below:

$$F_{ICF} = \frac{\Sigma\sigma_{ICF}}{\sigma_{TF}} \times 100. \quad (10)$$

The F_{ICF} for both the systems has been deduced at different energies and is plotted as a function of reduced projectile energy (E_{beam}/V_b, where V_b is Coulomb barrier of respective systems) in Figs. 9(a) and 9(b). The reduced projectile energy (E_{beam}/V_b) has been used to incorporate the effect of Coulomb barrier while comparing different projectile-target combinations in a plot. As can be seen from Fig. 9(a), at the threshold of ICF (i.e., ≈75 MeV in case of ^{16}O+^{169}Tm system) the relative percentage F_{ICF} is found to ≈10% of the total fusion cross section (σ_{TF}), which increases with projectile energy. At the highest studied energy (i.e., ≈95 MeV) the relative percentage of ICF fraction approaches to ≈30% of σ_{TF}. Similar energy dependence of ICF fraction for ^{16}O+^{159}Tb system has also been observed, where ICF fraction at ≈75 MeV is found to be ⩽1% of σ_{TF}, but at ≈95 MeV, it approaches to ≈20% of the total fusion cross section. Further, the percentage ICF contribution is an order of magnitude higher for ^{16}O+^{169}Tm system as compared to ^{16}O+^{159}Tb system at ≈75 MeV. However, it almost approaches to nearly the same value at higher energies. This may be because of the fact that as the beam energy increases, the effect of Coulomb barrier goes on diminishing. An attempt has also been made to estimate the similar energy dependent of F_{ICF} for ^{12}C+^{128}Te and ^{12}C+^{165}Ho systems studied earlier [3,27] and is shown in Fig. 9(b). The percent F_{ICF} for ^{12}C+^{165}Ho system is shown in the inset of Fig. 9(b) in order to see the variation more clearly. As can be seen from this figure, the incomplete fusion fraction for these systems also increases with the projectile energy. It may, however, be pointed out on the basis of Figs. 9(a) and 9(b) that the ICF fraction for ^{12}C and ^{16}O induced reactions increases with the charge and mass of target nucleus. Further, the difference between two systems at different projectile energies can be seen quite clearly, where the ICF fraction is found to be more for ^{16}O+^{169}Tm system than that for ^{16}O+^{159}Tb system, which shows the sensitiveness of ICF fraction to the mass asymmetry of interacting partners.

Mogenstern *et al.* [55], suggested that the onset of incomplete fusion is governed by the relative velocity ($v_{relative}$) of projectile (i.e., $\sqrt{2(E_{c.m.} - V_b)/\mu}$, here; V_b is the CB between the interacting partners, $E_{c.m.}$ is the projectile energy in center of mass system and μ is the reduced mass of the system) and mass asymmetry of the interacting partners. With this in view, the percentage F_{ICF} for ^{16}O+^{159}Tb, ^{16}O+^{169}Tm, ^{12}C+^{128}Te, and ^{12}C+^{165}Ho systems has been deduced at a constant value of $v_{relative}$. The mass asymmetry dependent percentage ICF fraction is shown in Fig. 10. As can be seen from this figure, in general, the data points suggest more ICF probability for more mass asymmetric systems than relatively mass symmetric system, which support the systematics presented by Morgenstern *et al.* [56]. However, the percentage ICF fraction for ^{16}O+^{169}Tm system is not following the general trend as inferred from the plot (Fig. 10). The above conflict in the measurements can be explained by considering projectile structure effect along with the mass asymmetry of interaction partners. As such, it can be pointed out that, for ^{16}O-induced reactions with ^{159}Tb and ^{169}Tm, percentage ICF fraction is more for mass asymmetric system. However, for ^{12}C-induced reactions with ^{128}Te and ^{165}Ho, the percentage F_{ICF} is also indicate the similar trends as that of ^{16}O-induced reactions. As such, it may not be out of order to state that, mass asymmetry is also a function of

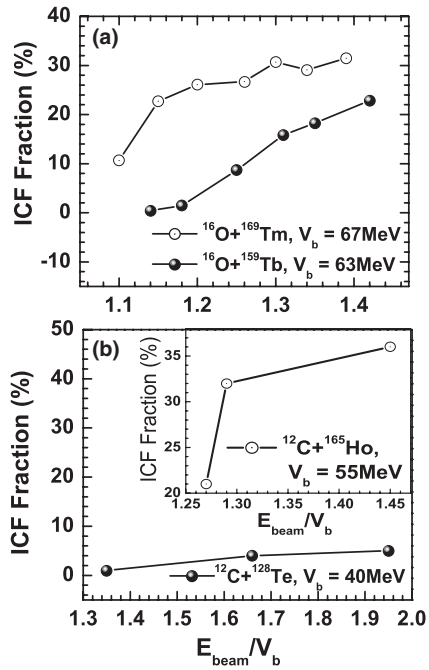

FIG. 9. Percentage incomplete fusion fraction (F_{ICF}) as a function of reduced projectile energy (E_{beam}/V_b) for (a) ^{16}O+^{159}Tb, ^{16}O+^{169}Tm and (b) ^{12}C+^{128}Te and ^{12}C+^{165}Ho (inset) systems.

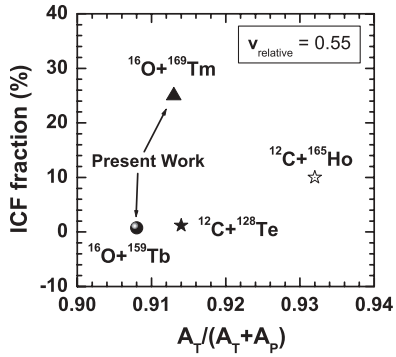

FIG. 10. Variation of percentage ICF fraction as a function of mass asymmetry of interacting partners at constant relative velocity ($v_{\text{relative}} = 0.55$) for different systems.

projectile structure. However, for better understanding of underlying processes, detailed measurements for various projectile-target combinations are required.

V. SUMMARY AND CONCLUSIONS

In this paper, some of the results of the experiments performed in order to study the influence of incomplete fusion on complete fusion process have been presented. Excitation functions for four radio-nuclides; ^{168m,167}Lu, ^{167}Yb, and ^{166}Tm produced in ^{16}O+^{159}Tb system, and five radio-nuclides; ^{179,177}Re, ^{177}W, ^{178}Ta, and ^{177}Hf produced in ^{16}O+^{169}Tm via complete and/or incomplete fusion in the energy range ≈75–95 MeV have been measured. The experimental data have been compared with the predictions of theoretical model code PACE2. The enhancement in the production cross sections, in case of α-emission channels (after correcting the precursor contribution, if any), as compared to PACE2 calculations has been attributed to the incomplete fusion reaction. The incomplete fusion fraction (F_{ICF}) is found to be $\leqslant$1% at ≈75 MeV, while, it is approaching ≈20% of the total fusion cross section (σ_{TF}) at ≈95 MeV for ^{16}O+^{159}Tb system. However, F_{ICF} is found to be ≈10% at ≈75 MeV and observed to be ≈30% of σ_{TF} at ≈95 MeV for ^{16}O+^{169}Tm system. It may however be pointed out that F_{ICF} is also found to be more in mass asymmetric systems than that of mass symmetric systems, though, the projectile structure effect appears to play a significant role in the systematics but this conjecture needs to be confirmed by further experimental data. The observation of large percentage F_{ICF} may be attributed to the prompt breakup of projectile into α-clusters (^{16}O $\Rightarrow$ ^{12}C+^{4}He and/or ^{8}Be^{8}Be), the probability of breakup increasing with the incident projectile energy. Hence, it may be inferred that, in general, the percentage F_{ICF} is sensitive for projectile energy, mass asymmetry of interacting partners (projectile structure effect apart). The percentage F_{ICF} have been found to increase with projectile energy. The present observations are thus in agreement with the Morgenstern systematics [56]. As such, it may be concluded that apart from complete fusion, the ICF is also a process of greater importance at these energies, and hence, while predicting the total reaction cross section, the contribution coming from incomplete fusion may also be taken into consideration. Moreover, in order to have better understanding of complete and incomplete fusion and perfect modeling of incomplete fusion processes, it would be quite interesting to perform more detailed experiments for different projectile-target combinations. The additional information can be obtained regarding the ICF processes by the measurement of spin distribution of residues populated by CF as well as ICF, using particle-γ coincidence technique both at relatively low and higher bombarding energies.

ACKNOWLEDGMENTS

The authors are thankful to Prof. Amit Roy, Inter-University Accelerator Center (IUAC), New Delhi, India for extending all the facilities for carrying out the experiments. Dr. R. K. Bhowmik and Prof. P. R. S. Gomes for several scientific discussions to improve this manuscript. Thanks are also due to Dr. S. Murlithar and Dr. R. P. Singh for their support and encouragement during the experiments. One of the authors (P.P.S.) thanks the IUAC for support and hospitality.

[1] F. Schussler, H. Nifenecker, B. Jakobsson, V. Kopljar, K. Soderstrom, S. Leray, C. Ngo, S. Souza, J. P. Bondorf, and K. Sneppen, Nucl. Phys. **A584**, 704 (1995).
[2] E. Gadioli, C. Brattari, M. Cavinato, E. Fabrici, E. Gadioli Erba, V. Allori, A. Di. Filippo, S. Vailati, T. G. Stevens, S. H. Connell, J. P. F. Sellschop, F. M. Nortier, G. F. Steyn, and C. Marchetta, Nucl. Phys. **A641**, 271 (1998).
[3] S. Gupta, B. P. Singh, M. M. Musthafa, H. D. Bhardwaj, and R. Prasad, Phys. Rev. C **61**, 064613 (2000).
[4] L. Corradi *et al.*, Phys. Rev. C **71**, 014609 (2005).
[5] M. Dasgupta, P. R. S. Gomes, D. J. Hinde, S. B. Moraes, R. M. Anjos, A. C. Berriman, R. D. Butt, N. Carlin, J. Lubian, C. R. Morton, J. O. Newton, and A. Szanto de Toledo, Phys. Rev. C **70**, 024606 (2004).
[6] S. Chakrabarty, B. S. Tomar, A. Goswami, G. K. Gubbi, S. B. Manohar, A. Sharma, B. B. Kumar, and S. Mukherjee, Nucl. Phys. **A678**, 355 (2000).
[7] D. J. Parker, J. Asher, T. W. Conlon, and I. Naqib, Phys. Rev. C **30**, 143 (1984).
[8] M. Cavinato, E. Fabrici, E. Gadioli, P. Vergani, M. Crippa, G. Colombo, I. Redaeli, and M. Ripamonti, Phys. Rev. C **52**, 2577 (1995).
[9] H. C. Britt and A. R. Quinton, Phys. Rev. **124**, 877 (1961).
[10] T. Inamura, M. Ishihara, T. Fukuda, T. Shimoda, and H. Hiruta, Phys. Lett. **B68**, 51 (1977).
[11] P. P. Singh, B. P. Singh, Unnati, B. Sharma, M. K. Sharma, R. Kumar, K. S. Golda, D. Singh, S. Muralithar, R. P. Singh, H. D. Bhardwaj, M. A. Ansari, R. Prasad, and R. K. Bhowmik, DAE-BRNS, Nucl. Phys. Sym. V **51**, 361 (2006).
[12] J. Wilczynski, K. Siwek-Wilczynaski, J. Van Driel, S. Gonggrijp, D. C. J. M. Hageman, R. V. F. Janssens, J. Lukasiak, R. H. Siemssen, and S. Y. Van der Werf, Nucl. Phys. **A373**, 109 (1982).
[13] T. Udagawa and T. Tamura, Phys. Rev. Lett. **45**, 1311 (1980).

[14] J. P. Bondrof, J. N. De, G. Fai, A. O. T. Karvinen, and J. Randrup, Nucl. Phys. **A333**, 285 (1980).
[15] W. Trautmann, O. Hansen, H. Tricoire, W. Hering, R. Ritzka, and W. Trombik, Phys. Rev. Lett. **53**, 1630 (1984).
[16] T. Inamura, T. Kjima, T. Nomura, T. Sugitate, and H. Utsunomiya, Phys. Lett. **B84**, 71 (1982).
[17] T. Inamura, A. C. Kahler, D. R. Zolnowski, U. Garg, T. T. Sugihara, and M. Wakai, Phys. Rev. C **32**, 1539 (1985).
[18] J. B. Natowitz, S. Leray, R. Lukas, C. Ngo, E. Tomasi, and C. Volant, Z. Phys. A **325**, 467 (1986).
[19] M. Blann *et al*., Phys. Rev. C **31**, 295 (1985).
[20] J. P. Bondrof *et al*., Nucl. Phys. **A333**, 285 (1980).
[21] D. H. E. Gross and J. Wilczynski, Phys. Lett. **B67**, 1 (1977).
[22] H. Tricoire *et al*., Z. Phys. A **312**, 221 (1983).
[23] H. C. Britt and A. R. Quinton, Phys. Rev. **124**, 877 (1961).
[24] K. Siwek-Wilczynska *et al*., Phys. Rev. Lett. **42**, 1599 (1979).
[25] S. Chakrabarty, B. S. Tomar, A. Goswami, G. K. Gubbi, S. B. Manohar, A. Sharma, B. B. Kumar, and S. Mukharjee, Nucl. Phys. **A678**, 355 (2000).
[26] P. Vergani, E. Gadioli, E. Vaciago, E. Fabrici, E. Gadioli Erba, M. Galmarini, G. Ciavola, and C. Marchetta, Phys. Rev. C **48**, 1815 (1993).
[27] M. K. Sharma, B. P. Singh, S. Gupta, M. M. Musthafa, H. D. Bhardwaj, and R. Prasad, J. Phys. Soc. Jpn. **72**, 1917 (2003).
[28] P. P. Singh, M. Phil. dissertation, A. M. University, Aligarh, India (2005), unpublished.
[29] S. Gupta, B. P. Singh, M. M. Musthafa, H. D. Bhardwaj, M. K. Sharma, R. Prasad, and A. K. Sinha, J. Phys. Soc. Jpn. **71**, 2434 (2002).
[30] D. J. Parker, J. J. Hogan, and J. Asher, Phys. Rev. C **39**, 2256 (1989).
[31] H. Morgenstern, W. Bohne, W. Galster, and K. Grabisch, Z. Phys. A **324**, 443 (1986).
[32] H. Morgenstern, W. Bohne, W. Galster, and K. Grabisch, Phys. Rev. Lett. **52**, 1104 (1984).
[33] M. F. Vineyard, J. S. Bauer, J. F. Crum, C. H. Gosdin, R. S. Trotter, D. G. Kovar, C. Beck, D. J. Henderson, R. V. F. Janssens, B. D. Wilkins, C. F. Maguire, J. F. Mateja, F. W. Prosser, and G. S. F. Stephens, Phys. Rev. C **45**, 1784 (1992).
[34] C. Beck, D. G. Kovar, S. J. Sanders, B. D. Wilkins, D. J. Henderson, R. V. F. Janssens, W. C. Ma, M. F. Vineyard, T. F. Wang, C. F. Maguire, F. W. Prosser, and G. Rosner, Phys. Rev. C **39**, 2202 (1989).
[35] P. Walker and G. Dracoulis, Nature (London) **399**, 35 (1999).
[36] S. M. Mullins *et al*., Phys. Lett. **B393**, 279 (1997).
[37] M. Kaci *et al*., Phys. Rev. C **56**, R600 (1997).
[38] C. Rubbia *et al*., Report CERN/AT/95-94(ET).
[39] M. M. Musthafa, M. K. Sharma, B. P. Singh, and R. Prasad, App. Rad. Isot. **62**, 419 (2005).
[40] M. K. Sharma, Unnati, B. K. Sharma, B. P. Singh, H. D. Bhardwaj, R. Kumar, K. S. Golda, and R. Prasad, Phys. Rev. C **70**, 044606 (2004).
[41] M. K. Sharma, Unnati, B. P. Singh, H. D. Bhardwaj, R. Kumar, K. S. Golda, and R. Prasad, Nucl. Phys. **A776**, 83 (2006).
[42] P. P. Singh, M. K. Sharma, Unnati, D. P. Singh, R. Kumar, K. S. Golda, B. P. Singh, and R. Prasad, Eur. Phys. J. A **34**, 29 (2007).
[43] J. K. Tuli, Nuclear Wallet Card, National Nuclear Data Center, Brookhaven National Laboratory, Upton, New York, USA (2000).
[44] B. P. Singh, Ph.D. thesis, A. M. University, Aligarh, India (1991), unpublished.
[45] E. Brown and R. B. Firestone, *Table of Isotopes* (Wiley, New York, 1986).
[46] A. Gavron, Phys. Rev. C **21**, 230 (1980).
[47] R. Bass, Nucl. Phys. **A231**, 45 (1985).
[48] F. D. Becchetti and G. W. Greenlees, Phys. Rev. **182**, 1190 (1969).
[49] G. R. Satcher, Nucl. Phys. **70**, 177 (1965).
[50] P. M. Endt *et al*., At. Data Nucl. Data Tables **26**, 47 (1981).
[51] J. P. Lestone, Phys. Rev. C **53**, 2014 (1996).
[52] A. Gilbert and A. G. N. Cameron, Can. J. Phys. **43**, 1446 (1965).
[53] K. S. Babu, R. Tripathi, K. Sudarshan, B. D. Srivastva, A. Gowswami, and B. S. Tomar, J. Phys. G **29**, 1011 (2003)
[54] P. R. S. Gomes, I. Padron, M. D. Rodriguez, G. V. Marti, R. M. Anjos, J. Lubian, R. Vegia, R. Liguori Neto, E. Crema, N. Added, L. C. Chamon, J. O. Fernadez Niello, O. A. Capurro, A. J. Pacheco, J. E. Testoni, D. Abriola, A. Arazi, M. Ramirez, and M. S. Hussein, Phys. Lett. **B601**, 20 (2004).
[55] H. Morgenstern, W. Bohne, K. Grabisch, H. Lehr, and W. Stoffler, Z. Phys. A **313**, 39 (1983).
[56] H. Morgenstern, W. Bohne, W. Galster, K. Grabisch, and A. Kyanowski, Phys. Rev. Lett. **52**, 1104 (1984).